Effect of Successive Alkylation of N,N −Dialkyl Amides on the Complexation Behavior of Uranium and Thorium: Solvent Extraction, Small Angle Neutron Scattering, and Computational St...

ARTICLE *in* THE JOURNAL OF PHYSICAL CHEMISTRY B · NOVEMBER 2014

Impact Factor: 3.3 · DOI: 10.1021/jp5074285 · Source: PubMed

THE JOURNAL OF PHYSICAL CHEMISTRY A

Article

pubs.acs.org/JPCA

Investigations on Preferential Pu(IV) Extraction over U(VI) by *N,N*-Dihexyloctanamide versus Tri-*n*-butyl Phosphate: Evidence through Small Angle Neutron Scattering and DFT Studies

P. K. Verma,[†] Neelam Kumari,[†] P. N. Pathak,*[,†] Biswajit Sadhu,[‡] Mahesh Sundararajan,[§] V. K. Aswal,[∥] and P. K. Mohapatra[†]

[†]Radiochemistry Division, [‡]Radiation Safety Systems Division, [§]Theoretical Chemistry Section, and [∥]Solid State Physics Division, Bhabha Atomic Research Centre, Trombay, Mumbai-400085, India

ABSTRACT: Straight chain amide *N,N*-dihexyloctanamide (DHOA) has been found to be a promising alternative extractant to tri-*n*-butyl phosphate (TBP) for the reprocessing of irradiated uranium- and thorium-based fuels. Unlike TBP, DHOA displays preferential extraction of Pu(IV) over U(VI) at higher acidities (≥3 M HNO_3) and poor extraction at lower acidities. Density functional theory (DFT) based calculations have been carried out on the structures and relative binding energies of U(VI) and Pu(IV) with the extractant molecules. These calculations suggest that the differential hardness of the two extractants is responsible for the preferential binding/complexation of TBP to uranyl, whereas the softer DHOA and the bulky nature of the extractant lead to stronger binding/complexation of DHOA to Pu(IV). In conjunction with quantum chemical calculations, small angle neutron scattering (SANS) measurements have also been performed for understanding the stoichiometry of the complex formed that leads to relatively lower extraction of Th(IV) (a model for Pu(IV)) as compared to U(VI) using DHOA and TBP as the extractants. The combined experimental and theoretical studies helped us to understand the superior complexation/extraction behavior of Pu(IV) over U(VI) with DHOA.

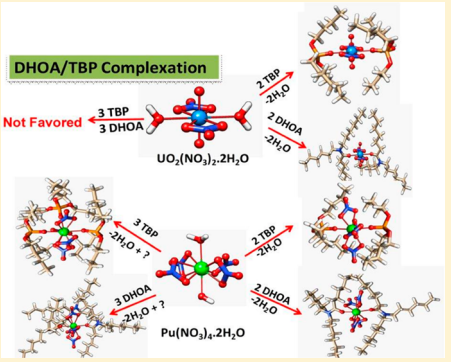

1. INTRODUCTION

Nuclear fuel cycle refers to the activities associated with the production of electricity by nuclear reactors. It starts with the mining and milling of uranium and ends with the disposal of nuclear waste. The reprocessing of used fuel and recycling of nuclear material for power generation is called a closed fuel cycle. To sustain a nuclear power program beyond the availability of naturally occurring uranium, it is imperative to follow the closed fuel cycle option. Even though the tri-*n*-butyl phosphate (TBP)-based PUREX (Plutonium Uranium Reduction EXtraction) process has been the workhorse of the nuclear fuel reprocessing industry for the decades, a few drawbacks such as the deleterious nature of degradation products (poor decontamination factor), non-incinerability (large secondary waste generation), solubility in aqueous stream (red oil formation), and the third-phase formation (tetravalent ions) associated with the use of this extractant have caused concern to separation scientists and technologists. In view of this, *N,N*-dialkyl aliphatic amides were proposed as alternative extractants for nuclear fuel reprocessing, since the work of Siddall.[1] Extensive efforts on the development of alternative extractants to TBP have shown that straight chain amides such as *N,N*-dihexyloctanamide (DHOA) (Figure 1) are promising alternatives for the reprocessing of irradiated uranium and thorium based fuels.[2−6] The liquid−liquid batch extraction studies have shown that U(VI) and Pu(IV) can be co-extracted living bulk of fission products in raffinate and hence can be employed in the PUREX process.[2,7] Np(V) alone has very poor or no extractability with TBP or DHOA, but if the feed contains appreciable amount of U(VI), Np(V) can be extracted to the organic phase because of the formation of a cation−cation complex of U(VI)−Np(V).[8] With tetravalent actinides such as Th(IV) or Pu(IV), both TBP and DHOA form a third phase, which refers to the splitting of the organic phase into diluents-rich and metal-extractant solvate-rich phases.[5,6] This is mainly guided by the species formed under the given experimental conditions. Verma et al. studied the effects of extractants and diluents on third-phase formation and showed

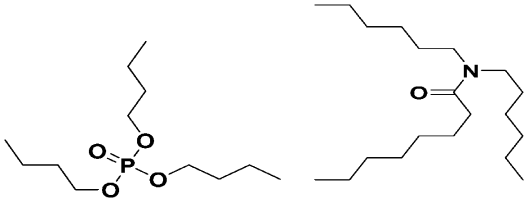

Fig.1(a): TBP Fig.1(b): DHOA

Figure 1. Structures of TBP and DHOA.

Received: March 27, 2014
Revised: May 8, 2014
Published: May 9, 2014

that dipole−dipole interaction between cores of a metal ligand reverse micelles causes their aggregation, which subsequently leads to third-phase formation, and such interaction is not favorable in polar diluents.[9]

TBP displays preference for the extraction of U(VI) over Pu(IV) from nitric acid medium. In contrast, DHOA shows higher affinity for Pu(IV) over U(VI) at higher acidities (≥3 M HNO_3) and reversal in the trend at lower acidities. This behavior has been explained earlier in terms of the change in the stoichiometry of the extracted species of Pu(IV) at lower (mono- or disolvated complexes) and higher acidities (trisolvated complex).[10] Similarly, the solvent extraction studies using DHOA suggested that the dialkylamides can be used as an extractant for the reprocessing of Th-based advanced heavy water reactor (AHWR) spent fuels.[5,6,11] This offers better extraction of U(VI) and Pu(IV) over Th(IV) from nitric acid medium. Even though the use of DHOA for reprocessing of U- and Th-based spent fuels appears to be promising, there is a need to investigate its preference for Pu(IV) over U(VI) (for U-based feed solutions) and for U(VI) and Pu(IV) over Th(IV) (for AHWR feed solutions). Most of the observations made by different groups on differences in the extraction behavior of the dialkylamides and organophosphorus extractants, e.g., third-phase formation, selectivity for particular metal ion, etc., can be explained if the nature of the complex formed under a given experimental condition is well known.[9,12−15] This can be studied either by advanced spectroscopic tools such EXAFS and mass spectrometry or by appropriate computational studies.[16−29] Quantum chemical methods have always played a crucial role in understanding the complexing/coordinative ability of various organic extractants and inorganic ions with actinyl ions. These studies provide structural information and the binding affinities under different experimental conditions.[22,24,25,27−29] Recently, we carried out density functional theory (DFT) based calculations to understand the third-phase formation of thorium with TBP and DHOA extractants.[9] In this manuscript, we adopted a similar computational strategy to understand the difference in their complexation and hence extraction behavior toward U(VI) and Pu(IV) ions even though both extractants have comparable acid uptake constants (K_H values).[30] In conjunction with quantum chemical calculations, small angle neutron scattering (SANS) measurements were performed to understand the changes in the stoichiometry of the extracted species of Pu(IV) and U(VI) with TBP and DHOA, which could help in understanding the relatively lower extraction of U(VI) as compared to Pu(IV) using DHOA as the extractant. It should be noted that no Pu(IV) sample was used for SANS measurements due to restriction at the experimental facility, and hence its tetravalent homologue Th(IV) was used. This work may provide a better insight into the understanding of complexation behavior of these ligands with the tetravalent and the hexavalent actinyl cations relevant to the reprocessing of nuclear waste.

2. EXPERIMENTAL SECTION

2.1. Materials. DHOA used in this work was synthesized at Radiochemistry Division, BARC as per the reported method.[31] Deuterated *n*-dodecane (dodecane-d_{26}, 98 atom % D, Aldrich), TBP (Heavy Water Board, India), and *n*-dodecane (Transware Chemia Handelsgesellschaft, Hamburg, Germany) were used without further purification. Other reagents used in this work were of AR grade. Sample solutions (1.1 M TBP/DHOA) were prepared by dissolving their required quantities in the deuterated diluent to obtain a better contrast for the aggregates formed in this study. Stock solutions of Th(IV) (8.6×10^{-3} M) and U(VI) (8.4×10^{-3} M) in 3 M HNO_3 were prepared by dissolving required weights of $Th(NO_3)_4 \cdot 5H_2O$ and UO_2, respectively. The organic phases were equilibrated in glass equilibration tubes (15 mL capacity) either with 3 M HNO_3 or with Th(IV)/U(VI) stock solutions at 3 M HNO_3 as per the requirements. These tubes were subsequently centrifuged, and the organic phases were separated from the aqueous phases. Table 1 provides the details of the organic samples used for the SANS studies.

Table 1. Details of Samples Used for the SANS Measurements[a]

sample	details
1	1.1 M TBP
2	1.1 M TBP/3 M HNO_3
3	1.1 M TBP/8.6×10^{-3} M Th(IV) 3 M HNO_3
4	1.1 M TBP/8.4×10^{-3} M U(VI) 3 M HNO_3
5	1.1 M DHOA
6	1.1 M DHOA/3 M HNO_3
7	1.1 M DHOA/8.6×10^{-3} M Th(IV) 3 M HNO_3
8	1.1 M DHOA/8.4×10^{-3} M U(VI) 3 M HNO_3

[a]Organic phase(s): 1.1 M TBP/1.1 M DHOA solutions in deuterated *n*-dodecane; temp 25 °C.

2.2. Computational Details. Geometry optimizations of all atoms were carried out within the framework of DFT. A BP86 functional in conjunction with the def2-SV(P) basis set was used for geometry optimizations and a B3LYP functional with the TZVP basis set for energetics.[32−38] To ease the computational cost, a relativistic small core effective core potential (ECP, 60 electrons at core) was used to treat the actinide ions, whereas the valence electrons were treated using the def-SV(P) basis set. All calculations were performed with ORCA 3.0 version.[39] The resolution of the identity (Split-RI-J) approximation was used in combination with the appropriate auxiliary basis set. The binding energies were corrected for solvent effects using COSMO continuum solvation models with dodecane as the solvent (ε = 2). The local hardness and polarizabilities of TBP, DHOA, U(VI), and Pu(IV) were calculated using the EPOLAR module as implemented in ORCA. The use of GGA functional for geometry optimizations is known to describe better geometric parameters for U and Pu complexes.[40−44] We used singlet and quintet multiplicities for uranyl and Pu(IV) complexes. A Mülliken charge scheme analysis was used to understand the preferential binding affinities of the two extractants.

2.3. SANS Measurements. SANS deals with the scattering of a monochromatic beam of neutrons from the sample, and the scattered neutron intensity is measured as a function of the scattering angle. The SANS diffractometer facility at the Dhruva reactor, BARC, Trombay was used for these measurements.[45] The mean wavelength of the incident neutron beam at this facility was 5.2 Å, having a resolution of ∼15%. The scattering wave vector (Q) range of the diffractometer was 0.017−0.35 $Å^{-1}$. The differential scattering cross-section per unit volume ($d\Sigma/d\Omega$) is measured as a function of Q. The sample is taken in the form of a plate to maintain a uniform thickness for the beam area as a function of the scattering vector. The measured intensity, $I(Q)$, is normalized to the differential scattering cross-section $d\sum/d\Omega(Q)$ using a standard procedure.[46] This

dx.doi.org/10.1021/jp503037q | J. Phys. Chem. A 2014, 118, 3996−4004

technique generally finds applications in understanding the material structure of sizes in the range of 10−200 Å. The Baxter sticky spheres model, based on the interaction between small particles, was employed to analyze the changes in scattering intensities of the organic samples used in the present work.

For a miceller system dispersed in a medium, $d\Sigma/d\Omega$ can be expressed as

$$\frac{d\Sigma}{d\Omega}(Q) = n(\rho_p - \rho_s)^2 V^2 P(Q) S(Q) \quad (1)$$

where n is the number density of the particles, ρ_p and ρ_s are, respectively, the scattering length densities of the particles and the medium, and V refers to the volume of the particle. The term $P(Q)$ was the intraparticle structure factor and was decided by the shape and size of the particle. On the other hand, $S(Q)$, the interparticle structure factor, depends on the spatial arrangement of particles and was, therefore, influenced by the interparticle interactions. However, the interparticle interference effects were negligible ($S(Q) \approx 1$) for dilute solutions, and therefore eq 1 can be simplified as

$$\frac{d\Sigma}{d\Omega}(Q) = n(\rho_p - \rho_s)^2 V^2 P(Q) \quad (2)$$

The value of $P(Q)$ for a spherical particle of radius R is expressed by

$$P(Q) = \left[\frac{3\{\sin(QR) - QR\cos(QR)\}}{(QR)^3}\right]^2 \quad (3)$$

For prolate ellipsoidal, $P(Q)$ is given by

$$P(Q) = \int_0^1 [F(Q,\mu)^2 d\mu] \quad (4)$$

$$F(Q,\mu) = \frac{3(\sin x - x\cos x)}{x^3} \quad (5)$$

x was defined by the following equation:

$$x = Q[a^2\mu^2 + b^2(1-\mu^2)]^{1/2} \quad (6)$$

where a and b are the semi-major and semi-minor axes of the ellipsoidal micelle, respectively, and μ is the cosine of the angle between the directions of a and the wave vector transfer, Q. The value of $S(Q)$ (eq 1) was calculated assuming attractive interaction between the particles using Baxter's sticky hard-sphere model. In this model, particles interact via a thin attractive square-well potential of depth U_0 (< 0) and width Δ. The basic results of the model are derived as the lowest order solution of the Ornstein−Zernike equation and Percus−Yevick closure relation. The expression for the structure factor is generally given by

$$S^{-1}(Q) = A^2(Q) + B^2(Q) \quad (7)$$

$$A(Q) = 1 + 12\eta\left(\alpha\frac{s(k) - kc(k)}{k^3} + \beta\frac{1-c(k)}{k^2} - \frac{\lambda}{12}\frac{s(k)}{k}\right) \quad (8)$$

$$B(Q) = 12\eta\left(\alpha\left[\frac{1}{2k} - \frac{s(k)}{k^2} + \frac{1-c(k)}{k^3}\right] + \beta\left[\frac{1}{k} - \frac{s(k)}{k^2}\right] - \frac{\lambda}{12}\frac{1-c(k)}{k}\right) \quad (9)$$

where $s(k) \equiv \sin(k)$, $c(k) \equiv \cos(k)$, $k \equiv Q(\sigma + \Delta)$, and

$$\alpha = \frac{1 + 2\eta - \mu'}{(1-\eta)^2}, \quad \beta = \frac{-3\eta + \mu'}{2(1-\eta)^2},$$
$$\mu' = \lambda'\eta(1-\eta)$$
$$\lambda' = \frac{6}{\eta}[\delta - (\delta^2 - \nu)^{1/2}], \quad \delta = \tau + \frac{\eta}{1-\eta},$$
$$\nu = \eta\frac{1 + \eta/2}{3(1-\eta)^2}$$

The parameter $\eta = \pi n(\sigma + \Delta)^3/6$ represents the effective "volume fraction", which depends on the potential width, Δ. The stickiness parameter (τ) is related to the potential parameters (U_0, Δ, σ) and temperature (T) as

$$\tau = \frac{\sigma + \Delta}{12\Delta}\exp\left(\frac{U_0}{k_B T}\right) \quad (10)$$

where k_B is Boltzmann's constant. For the particle interaction model calculations, the diameter of the micelles (σ), width of the square well attraction potential (Δ), depth of square-well potential (U_0), and stickiness parameter (τ) were used. It was important to mention that when the distance between the two particles is larger than σ but smaller than $\sigma + \Delta$, the particles experience attraction. The Baxter model approximation has been used to derive analytical expressions for the structure factor $S(Q)$.

3. RESULTS AND DISCUSSION

3.1. U(VI) and Th(IV) Complexation with TBP/DHOA: SANS Results. The SANS studies were carried out using 1.1 M TBP and 1.1 M DHOA in deuterated *n*-dodecane (dielectric constant, ε = 2.0 at 20 °C) medium (Table 1). Figures 2 and 3 show the variation in the differential scattering cross-section per unit volume ($d\Sigma/d\Omega$) as a function of the scattering vector, Q, before and after complexation of the metal ions (such as U(VI) and Th(IV)) with TBP and DHOA. SANS studies of fresh and 3 M HNO_3 equilibrated TBP/DHOA was also done for comparison purpose. It was evident that even though the

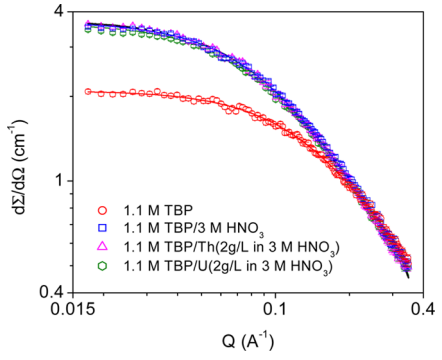

Figure 2. SANS data for 1.1 M TBP solution in deuterated *n*-dodecane.

dx.doi.org/10.1021/jp503037q | J. Phys. Chem. A 2014, 118, 3996−4004

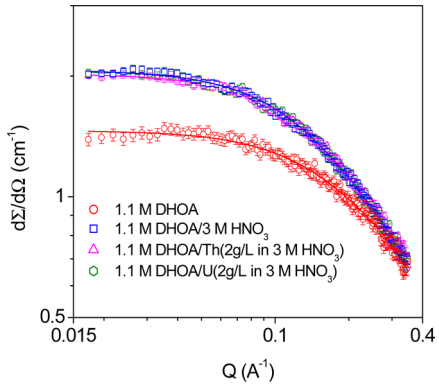

Figure 3. SANS data for 1.1 M DHOA solution in deuterated *n*-dodecane.

complexation studies were carried out under identical conditions, the two complexes differed in their stoichiometries. The dΣ/dΩ values for TBP/DHOA equilibrated with 3 M HNO_3 and U(VI)·TBP/U(VI)·DHOA and Th(IV)·TBP/Th(IV)·DHOA complex was comparable but higher than that for the pure TBP/DHOA as expected. Our previous study has shown that only a particle growth model gives very large values of aggregation number (N), which is hard to visualize even in the samples having third phases due to high metal loadings. Therefore, the scattering data in the present study was interpreted using the Baxter sticky spheres model. Table 2 lists the various fitted parameters for the present system using the Baxter sticky spheres model. There is no significant enhancement in stickiness parameter (τ^{-1}) values for the metal-loaded organic phases as compared to the corresponding fresh solvents (Table 2). This indicates that there is no increase in the short-range attractive forces between the polar cores of the metal−ligand aggregates due to dipole−dipole interactions. The metal−ligand aggregates are subjected to two opposing physical forces: (a) the thermal energy (k_BT) keeps the micelles dispersed in the diluents, and (b) the intermicellar attraction energy compels the micelles to stick together. The organic phase will be stable as long as these two opposing forces are balanced, or else aggregation will take place. The τ values of different samples were used to calculate the attractive potential energy (U_0) in k_BT units. It is evident that the attractive potential energies are comparable to those of the fresh solvents, suggesting that aggregation is not significant. Hence the fitted data can be assigned the stoichiometry of te complex formed. The stoichiometries of the complex formed are 1:2 and 1:3 for U(VI) and Th(IV), respectively, with either TBP or DHOA, which is in line with the conventional ligand variation/slope analysis methods used to find out stoichiometries of extracted species and was also supported by the computational studies (*vide infra*).

3.2. Theoretical Results. Actinyl complexes can exist in various stoichiometries. Even for a simple aqua-complex of uranyl cation ($UO_2(H_2O)_n$), Cao and Balasubramanian have shown that both n = 5 and 6 coordination complexes are preferred.[47] In this paper, we considered two nitrates equatorially coordinated to the uranyl (UO_2^{2+}) ion, whereas four nitrates are found to coordinate to the Pu(IV) ion. For both actinide ions, two water molecules were used to complete the coordination shell of the uranyl and Pu(IV) species. The optimized geometric parameters are listed in Table 3 for uranyl and Pu(IV) aqueous nitrate and for further complexation with TBP/DHOA and are very close to experimental data and previously performed computations,[48−54,57−59] which raises confidence in our computational methods applied here. The optimized value of the axial U═O bond length (U═O_{yl}) in uranyl nitrate hexahydrate was 1.79 Å (Table 3), which is slightly larger than U═O_{yl} (1.76 Å) of aqua uranyl cation.[55,56] As expected, the nitrates (~2.4 Å) are strongly bound to the actinides as compared to neutral water molecules (~2.5 Å). The optimized geometric parameters for $UO_2(NO_3)_2$·2TBP are very close to the experimental data obtained by EXAFS studies, which gives confidence in our computational methods used to predict TBP/DHOA complexation with U(VI) and Pu(IV).[52,53]

3.2.1. Complexation/Binding of TBP and DHOA with Uranyl Cation. The complexation/binding of the two extractants to uranyl can occur upon replacing the weakly bound water molecules. Prior to the binding of the two extractants, the axial U═O_{yl} bond length is 1.79 Å, which is in close agreement with the experimental data.[51−53] Replacement of the weakly bound inner sphere water molecules by TBP or DHOA leads to a small elongation of the U═O_{yl} bond length (1.80 Å, Figures 4, 5, and 6 or Table 3). TBP and DHOA coordinate through their phosphoryl and carbonyl groups respectively, forming 1:2 (metal/ligand) complexes in both the cases, which is also evident from our SANS studies. Further, both TBP and DHOA are strongly interacting to uranyl (2.35−2.37 Å), whereas the nitrates still interact in a bidentate mode (~2.5 Å). However, between DHOA and TBP, the interaction of TBP is somewhat stronger (2.35 vs 2.37 Å), and the nitrates have an asymmetric bidentate motif with TBP as compared to DHOA due to less steric hindrance and the hard nature of the TBP extractant, which can interact with similar hard U(VI) as compared to DHOA. The computed binding affinities of TBP

Table 2. Aggregation Number (N) Calculation on Different Samples Using Sticky Spheres Model[a]

sample	system	radius, R (Å)	volume fraction, ϕ	aggregation number, N	stickiness parameter, $1/\tau$	potential energy, U_0 (k_BT units)
1	1.1 M TBP	4.77	0.301	1.0	6.7	−0.90
2	1.1 M DHOA	5.21	0.395	1.0	5.5	−0.75
3	1.1 M TBP/3 M HNO_3	4.77	0.301	1.0	8.3	−1.18
4	1.1 M DHOA/3 M HNO_3	5.21	0.395	1.0	7.1	−1.05
5	1.1 M TBP Th (2 g/L in 3 M HNO_3)	6.87	0.301	3.0	7.1	−1.23
6	1.1 M DHOA Th (2 g/L in 3 M HNO_3)	7.51	0.395	3.0	5.1	−0.94
7	1.1 M TBP U (2 g/L in 3 M HNO_3)	6.01	0.301	2.0	7.5	−1.20
8	1.1 M DHOA U (2 g/L in 3 M HNO_3)	6.53	0.395	2.0	5.9	−1.02

[a]Organic phase(s): 1.1 M TBP/1.1 M DHOA solutions in *n*-dodecane; temp 25 °C.

dx.doi.org/10.1021/jp503037q | J. Phys. Chem. A 2014, 118, 3996−4004

Table 3. Optimized Values of Coordinative Distances in Different Complexes of Pu(IV) and Uranium with TBP and DHOA[a]

	$Pu(NO_3)_4{\cdot}2H_2O$	$Pu(NO_3)_4{\cdot}(H_2O)L$	$Pu(NO_3)_4{\cdot}L_2$	$Pu(NO_3)_4{\cdot}L_3$
$M-O_H$	2.49 Å	2.51 (2.52) Å		
$M-O_N$	2.40–2.44 Å	2.40–2.47 (2.39–2.48) Å	2.42–2.49 (2.44–2.49) Å	2.46–2.61 (2.29–3.96) Å
$M-O_E$		2.27 (2.26) Å	2.28–2.33 (2.29) Å	2.34, 2.34, 2.36 (2.32, 2.38, 2.39) Å
	$UO_2(NO_3)_2{\cdot}2H_2O$	$UO_2(NO_3)_2{\cdot}(H_2O)L$	$UO_2(NO_3)_2{\cdot}L_2$	
$M-O_{ax}$	1.79 Å	1.80 (1.79) Å	1.80 (1.80) Å	
$M-O_H$	2.54 Å	2.56 (2.56) Å		
$M-O_N$	2.48 Å	2.48–2.51 (2.47–2.51) Å	2.51–2.53 (2.51) Å	
$M-O_E$		2.33 (2.35) Å	2.33 (2.37) Å	

[a]$M-O_{H/N/E}$ = metal center–oxygen of H_2O, NO_3, or extractant (TBP or DHOA). Values outside the brackets are for TBP–metal complexe,s and those inside the brackets are for DHOA–metal complexes.

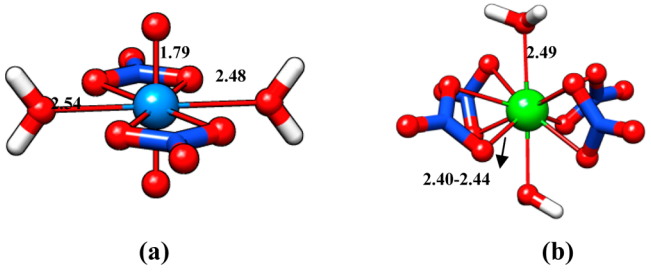

Figure 4. Optimized structures of (a) uranyl(VI) and (b) plutonium-(IV) nitrate dihydrate.

and DHOA are shown in Table 4. For both TBP and DHOA, we note that the binding affinity of the second molecule is somewhat less strong as compared to the first molecule binding to it. Between the two extractants, we find that TBP binding to uranyl is somewhat stronger (by 7–10 kcal mol^{-1}) as compared to DHOA, which is consistent with our experimental data, It should be noted that due to the presence of axial oxygens, more than two molecules of extractant cannot directly interact with the uranyl ion, hence restricting the stoichiometry of complex formed to1:2 (metal/ligand) for both the extractants.

3.2.2. Complexation/Binding of TBP and DHOA with Pu(IV). TBP and DHOA coordinate through their phosphoryl and carbonyl group, respectively, to Pu(IV) also, but forming 1:3 (metal/ligand) complex in both the cases, which is also observed in SANS studies. Unlike the case of the uranyl system, we observed some very interesting geometric and energetic trends for the binding of the two extractants to Pu(IV). In the optimized plutonium nitrate, we found that four nitrates were bound in the equatorial planes, whereas the two weakly bound water molecules (~2.50 Å) were located at axial positions. Both

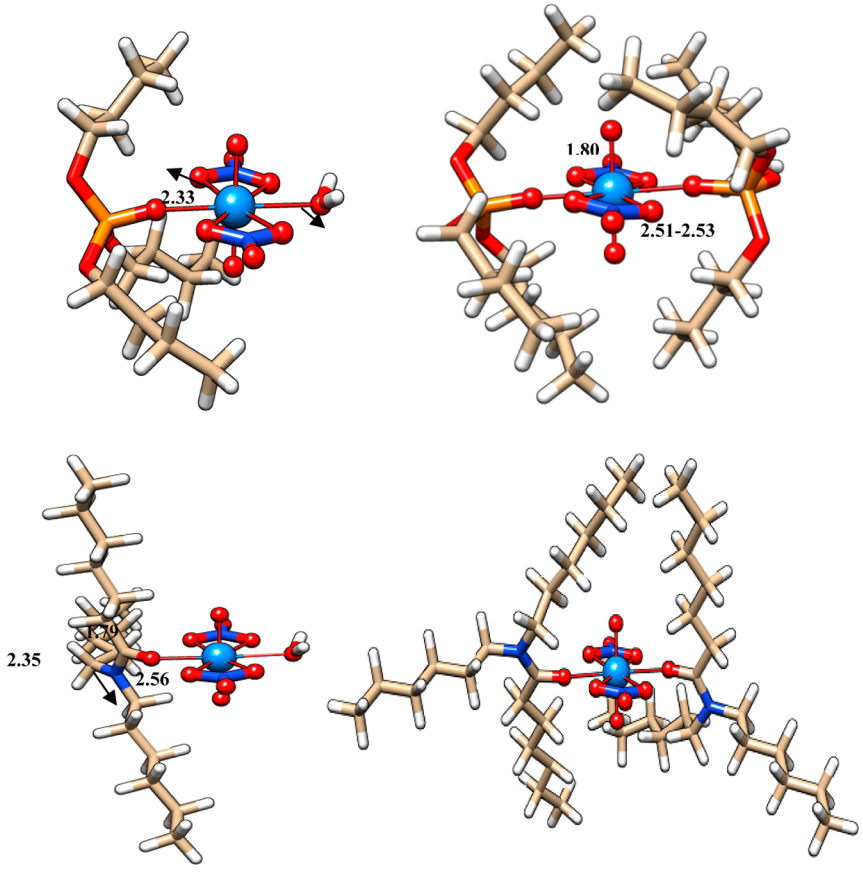

Figure 5. Optimized structures of uranyl(VI) nitrate with TBP and DHOA extractants.

dx.doi.org/10.1021/jp503037q | J. Phys. Chem. A 2014, 118, 3996–4004

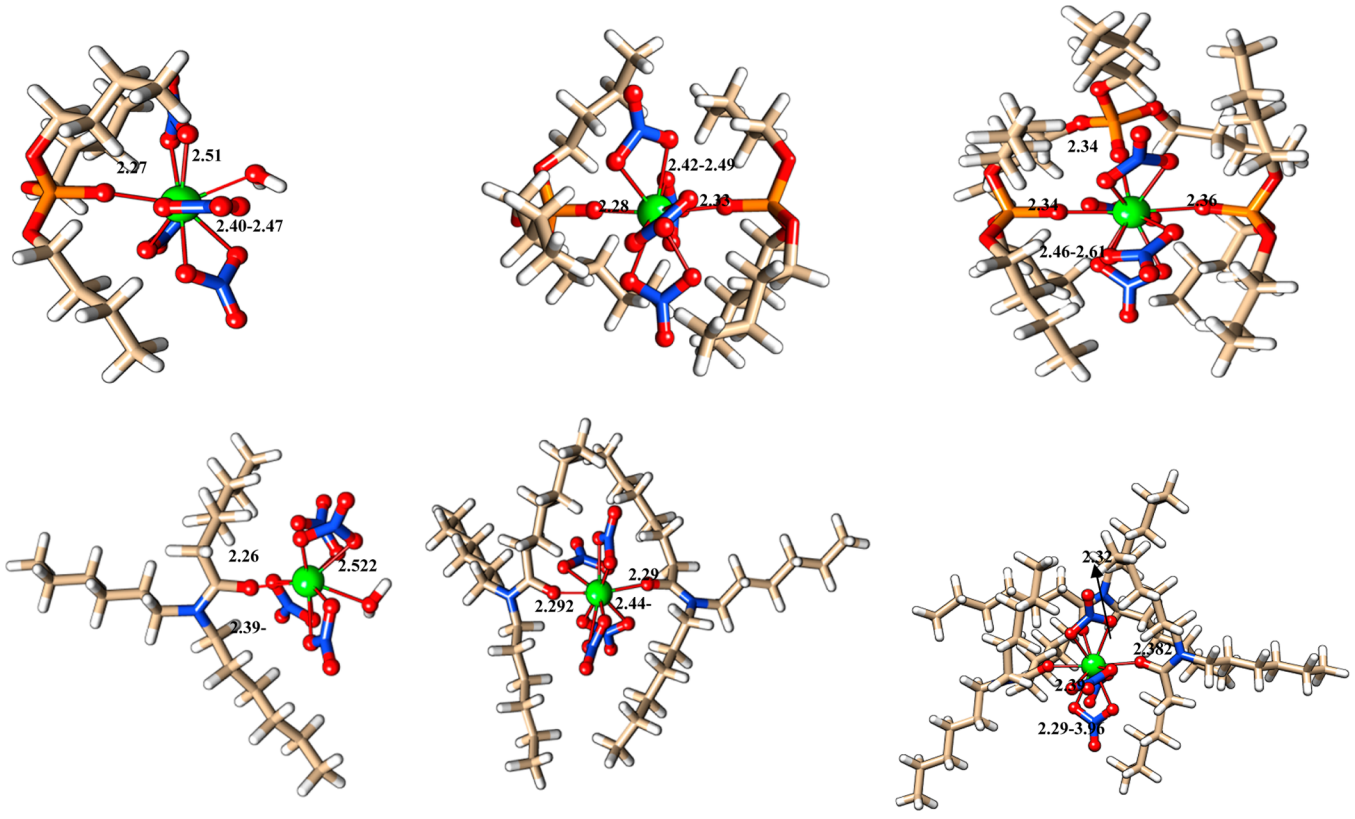

Figure 6. Optimized structures of plutonium(IV) nitrate with TBP and DHOA extractants.

Table 4. Calculated Binding Affinities (BE, kcal mol^{-1}) of TBP and DHOA Extractants with $UO_2(NO_3)_2{\cdot}2H_2O$ and $Pu(NO_3)_4{\cdot}2H_2O$

radionuclide−extractant reaction	BE (kcal mol^{-1})
$[UO_2(NO_3)_2{\cdot}2H_2O] + TBP \rightarrow [UO_2(NO_3)_2{\cdot}TBP{\cdot}H_2O] + H_2O$	−27.40
$[UO_2(NO_3)_2{\cdot}TBP{\cdot}H_2O] + TBP \rightarrow [UO_2(NO_3)_2{\cdot}2TBP] + H_2O$	−21.18
$[Pu(NO_3)_4{\cdot}2H_2O] + TBP \rightarrow [Pu(NO_3)_4{\cdot}TBP{\cdot}H_2O] + H_2O$	−29.51
$[Pu(NO_3)_4{\cdot}TBP{\cdot}H_2O] + TBP \rightarrow [Pu(NO_3)_4{\cdot}2TBP] + H_2O$	−24.77
$[Pu(NO_3)_4{\cdot}2TBP] + TBP \rightarrow [Pu(NO_3)_4{\cdot}3TBP]$	−37.83
$[UO_2(NO_3)_2{\cdot}2H_2O] + DHOA \rightarrow [UO_2(NO_3)_2{\cdot}DHOA{\cdot}H_2O] + H_2O$	−17.85
$[UO_2(NO_3)_2{\cdot}DHOA{\cdot}H_2O] + DHOA \rightarrow [UO_2(NO_3)_2{\cdot}2DHOA] + H_2O$	−13.69
$[Pu(NO_3)_4{\cdot}2H_2O] + DHOA \rightarrow [Pu(NO_3)_4{\cdot}DHOA{\cdot}H_2O] + H_2O$	−23.76
$[Pu(NO_3)_4{\cdot}DHOA{\cdot}H_2O] + DHOA \rightarrow [Pu(NO_3)_4{\cdot}2DHOA] + H_2O$	−14.94
$[Pu(NO_3)_4{\cdot}2DHOA] + DHOA \rightarrow [Pu(NO_3)_4{\cdot}3DHOA]$	−38.07

TBP and DHOA ligands were more strongly bound (by 0.1 Å) to Pu(IV) as compared to uranyl, which was probably due to stronger electrostatic interaction of the Pu^{4+} ion with the extractant molecules as compared to the uranyl ion. Furthermore, replacement of the inner sphere water molecule by TBP or DHOA led to weakening of prebound nitrate (2.40−2.47 Å). The computed binding affinity of TBP with Pu^{4+} was stronger as compared to DHOA (by ∼5 kcal mol^{-1}). Addition of a second molecule of TBP or DHOA leads to further weakening of the nitrate ion bonded (2.42−2.49 Å) to the Pu(IV). As compared to DHOA, TBP binds to Pu(IV) somewhat stronger by both 1:1 and 1:2 stoichiometries (Table 4). As expected, the binding strength of the second molecule of the extractant is weaker as compared to the first molecule binding, which is similar to those observed for uranyl binding to TBP and DHOA. However, addition of a third DHOA or TBP leads to a further elongation of the prebound nitrate ion, which becomes monodentate for the case of DHOA (2.29−3.96 Å) and strongly asymmetric for TBP (2.46−2.61 Å). This particular feature is particularly larger for DHOA as compared to TBP due to the bulkiness of the ligands. These changes in the geometry lead to the stronger binding of DHOA (>38 kcal mol^{-1}) as compared to TBP.

The actinide elements are classified as hard acids, especially in their higher oxidation states. The interaction of the ligands with an actinide center is conventional acid−base interaction in which the ligand serves as electron donor (base) to a vacant acceptor orbital of the metal (acid). As hard acids, actinide ions prefer to coordinate with hard bases; in view of this, we have computed the hardness (η) and polarizability (α) of the two extractants and the two actinide ions to understand these interactions, which further leads to the complexation between them. We have noted that U(VI) (η 308.24) and TBP (η 200.66) are more hard as compared to Pu(IV) (η 159.21) and DHOA (η 158.54), which certainly helps to understand the preferential binding of DHOA to Pu(IV) as compared to

dx.doi.org/10.1021/jp503037q | J. Phys. Chem. A 2014, 118, 3996−4004

U(VI) (Table 5) and hence the preferential extraction of Pu(IV) by DHOA. However, due to the bulky nature of DHOA, the steric effects complicate the binding affinities predictions. These findings are in line with those of Adamo et al., who reported that steric effects complicate the binding energy predictions.[60]

Table 5. Computed Polarizability (α) and Hardness (η, kcal mol^{-1}) of the Ligands and Metal Systems

	α	η
	Metal Ion	
U(VI)	4.98	308.24
Pu(IV)	6.91	159.21
	Extractant	
TBP	183.4	200.66
DHOA	249.7	158.54

The Mulliken charges on the individual fragments of the actinide complexes were computed to understand the charge transfer/acceptor properties of ligands/metal ions. As observed during the optimization studies, the addition of a third DHOA or TBP leads to further elongation of the prebound nitrate and now becomes monodentate for the case of DHOA and strongly asymmetric for TBP. So it was of interest to understand the role of the electrostatic forces in governing such an elongation or coordinating behavior of ligands/nitrates. In Table 6, we have listed the Mulliken charges on the individual fragments of the actinide complexes. As compared to DHOA, the extent of the charge transfer is more for TBP. However, the charge does not necessarily go to the metal ion, but rather to the uranyl oxygens, which is seen in other uranyl complexes.[44,61] This may probably be due to the covalent nature of uranyl oxygens as commonly observed in transition metal coordination complexes. However, for Pu^{4+}, DHOA charges are more transferred to the nitrates as compared to Pu itself, which leads to electrostatic repulsion with the metal making the nitrates monodentate. This monodentate nature facilitates the stronger binding of DHOA leading to large binding energies.

4. CONCLUSIONS

SANS and DFT studies have been carried out on the structures and relative binding energies of U(VI) and Pu(IV) with TBP and DHOA. Our calculations suggest that the differential hardness of the two extractants leads to the preferential binding/complexation of TBP to uranyl, whereas the softer DHOA and the bulky nature of the extractant lead to stronger binding/complexation of DHOA to Pu(IV). In conjunction with quantum chemical calculations, SANS measurements have been performed for understanding the stoichiometry of the complexes formed, which leads to relatively lower extraction of Th(IV) (a model for Pu(IV)) as compared to U(VI) using DHOA and TBP as the extractants. Thus, our computational results provide structural evidence for the possible and differential complexation/binding affinities of extractants to U(VI) and Pu(IV) nitrates. Although both TBP and DHOA bind strongly to the uranyl and the Pu(IV) ions for lower stoichiometric ratios, the binding of Pu(IV) with DHOA is stronger due to the change in the coordination mode of the nitrate ion from bidentate to monodentate. These studies explained the better extraction of Pu(IV) over U(VI) and poor extraction of Th(IV) for DHOA as compared to TBP. The combined experimental and theoretical studies helped us to understand the better complexation and hence extraction behavior of Pu(IV) over U(VI) using DHOA as extractant as compared to TBP.

AUTHOR INFORMATION

Corresponding Author

*Fax: 91-22-25505151. E-mail: ppathak@barc.gov.in.

Notes

The authors declare no competing financial interest.

ACKNOWLEDGMENTS

The authors thank Dr. A. Goswami, Head, Radiochemistry Division, Bhabha Atomic Research Centre, Mumbai, India, for his support and encouragement in this work. B.S. thanks Mr. Rajvir Singh, Dr. K. S. Pradeepkumar and Dr. D. N. Sharma for their constant support.

REFERENCES

(1) Siddall, T. H., III *Applications of Amides As Extractants*; USAEC Report DP-541, 1961.

(2) Pathak, P. N.; Kanekar, A. S.; Prabhu, D. R.; Manchanda, V. K. Recent R&D Studies Related to Coprocessing of Spent Nuclear Fuel Using *N,N*-dihexyloctanamide. *Sep. Sci. Technol.* **2009**, *44*, 3650−3663.

(3) Manchanda, V. K.; Pathak, P. N. Amides and Diamides As Promising Extractants in the Back End of the Nuclear Fuel Cycle: An Overview. *Sep. Purif. Technol.* **2004**, *35*, 85−103.

(4) Musikas, C. Completely Incinerable Extractants for the Nuclear Industry - A Review. *Min. Process. Extr. Metal. Rev.* **1997**, *17*, 109−142.

(5) Verma, P. K.; Kumari, N.; Prabhu, D. R.; Pathak, P. N. Optimization Studies for the Recovery of Thorium From Advanced

Table 6. Computed Mulliken Charges (au)

species	metal	axial O (U═O)	nitrate	ligand	water
$[Pu(NO_3)_4{\cdot}2H_2O]$	0.569		−0.171		0.556
$[Pu(NO_3)_4{\cdot}TBP{\cdot}H_2O]$	0.494		−1.064	0.270	0.299
$[Pu(NO_3)_4{\cdot}(TBP)_2]$	0.521		−1.047	0.526	
$[Pu(NO_3)_4{\cdot}(TBP)_3]$	0.598		−1.136	0.537	
$[Pu(NO_3)_4{\cdot}DHOA{\cdot}H_2O]$	0.523		−1.124	0.306	0.295
$[Pu(NO_3)_4{\cdot}(DHOA)_2]$	0.515		−1.139	0.624	
$[Pu(NO_3)_4{\cdot}(DHOA)_3]$	0.622		−1.222	0.601	
$[UO_2(NO_3)_2{\cdot}2H_2O]$	0.233	−0.121	−0.620		0.508
$[UO_2(NO_3)_2{\cdot}TBP{\cdot}H_2O]$	0.270	−0.156	−0.622	0.240	0.268
$[UO_2(NO_3)_2{\cdot}(TBP)_2]$	0.211	−0.186	−0.607	0.582	
$[UO_2(NO_3)_2{\cdot}DHOA{\cdot}H_2O]$	0.238	−0.156	−0.663	0.309	
$[UO_2(NO_3)_2{\cdot}(DHOA)_2]$	0.283	−0.184	−0.641	0.542	

Heavy Water Reactor High Level Waste (AHWR-HLW) Solutions Using Green Solvents. *Sep. Sci. Technol.* **2013**, *48*, 626−633.
(6) Pathak, P. N. *N,N*-Dialkyl Amides As Extractants For Spent Fuel Reprocessing: An Overview. *J. Radioanal. Nucl. Chem.* **2014**, *300*, 7−15.
(7) Statton, M. A.; Thompson, M. C. *Flowsheet for Coprocessing Uranium and Plutonium*; USDOE report DP-1505, 1979.
(8) Verma, P. K.; Pathak, P. N.; Bhattacharyya, A.; Prabhu, D. R.; Mohapatra, P. K. A Revisit of the Cation−Cation Interactions between Npo_2^+ and UO_2^{2+} In Nitric Acid Medium and Their Impact on Separation Processes: Spectrophotometric and Solvent Extraction Studies. *Dalton Trans.* **2013**, *42*, 14058−14063.
(9) Verma, P. K.; Pathak, P. N.; Mohapatra, P. K.; Aswal, V. K.; Sadhu, B.; Sundararajan, M. An Insight into Third-Phase Formation during the Extraction of Thorium Nitrate: Evidence for Aggregate Formation from Small Angle Neutron Scattering and Validation by Computational Studies. *J. Phys. Chem. B* **2013**, *117*, 9821−9828.
(10) Pathak, P. N.; Prabhu, D. R.; Kanekar, A. S.; Manchanda, V. K. Distribution Studies on Th(IV), U(VI) and Pu(IV) using Tri-n-Butylphosphate and *N,N*-Dialkyl Amides. *Radiochim. Acta* **2006**, *94*, 193−198.
(11) Kumari, N.; Prabhu, D. R.; Kanekar, A. S.; Pathak, P. N. Validation of Solvent Extraction Scheme for the Reprocessing of Advanced Heavy Water Reactor Spent Fuel Using *N,N*-Dihexyl Octanamide as Extractant. *Ind. Eng. Chem. Res.* **2012**, *51*, 14535−14542.
(12) Kumari, N.; Pathak, P. N.; Prabhu, D. R.; Manchanda, V. K. Comparison of Extraction Behavior of Neptunium from Nitric Acid Medium Employing Tri-*n*-Butyl Phosphate and *N,N*-dihexyl Octanamide as Extractants. *Sep. Sci. Technol.* **2012**, *47* (10), 1492−1497.
(13) Vasudeva Rao, P. R.; Kolarik, Z. A Review of Third Phase Formation in Extraction of Actinides by Neutral Organophosphorus Extractants. *Solvent Extr. Ion Exch.* **1996**, *14*, 955−993.
(14) Xiao, C.-L.; Wang, C.-Z.; Yuan, L.-Y.; Li, B.; He, H.; Wang, S.; Zhao, Y.-L.; Chai, Z.-F.; Shi, W.-Q. Excellent Selectivity for Actinides with a Tetradentate 2,9-Diamide-1,10-Phenanthroline Ligand in Highly Acidic Solution: A Hard−Soft Donor Combined Strategy. *Inorg. Chem.* **2014**, *53* (3), 1712−1720.
(15) Bhattacharyya, A.; Ghanty, T. K.; Mohapatra, P. K.; Manchanda, V. K. Selective Americium(III) Complexation by Dithiophosphinates: A Density Functional Theoretical Validation for Covalent Interactions Responsible for Unusual Separation Behavior from Trivalent Lanthanides. *Inorg. Chem.* **2011**, *50* (9), 3913−3921.
(16) Lucks, C.; Rossberg, A.; Tsushima, S.; Foerstendorf, H.; Scheinost, A. C.; Bernhard, G. Aqueous Uranium(VI) Complexes with Acetic and Succinic Acid: Speciation and Structure Revisited. *Inorg. Chem.* **2012**, *51* (22), 12288−12300.
(17) Visser, A. E.; Jensen, M. P.; Laszak, I.; Nash, K. L.; Choppin, G. R.; Rogers, R. D. Uranyl Coordination Environment in Hydrophobic Ionic Liquids: An in Situ Investigation. *Inorg. Chem.* **2003**, *42* (7), 2197−2199.
(18) Yaita, T.; Narita, H.; Suzuki, S.; Tachimori, S.; Shiwaku, H.; Motohashi, H. Structural Study of Holmium (III) and Uranium (VI) Organic Ligand Complexes By Extended X-Ray Absorption Fine-Structure Spectroscopy. *J. Alloys Compounds* **1998**, No. 271−273, 184−188.
(19) Verma, P. K.; Pathak, P. N.; Jayasekharan, T.; Vatsa, R. K.; Mohapatra, P. K. Characterization of the Species Formed during the Extraction of Thorium Employing Tri-*n*-butyl Phosphate and *N,N*-Dihexyl Octanamide as Extractants by Laser Desorption/Ionization - Time of Flight Mass Spectrometry. *Eur. J. Mass Spectrom.* **2013**, *19* (4), 275−283.
(20) Gresham, G. L.; Dinescu, A.; Benson, M. T.; Stipdonk, M. J. V.; Groenewold, G. S. Investigation of Uranyl Nitrate Ion Pairs Complexed with Amide Ligands Using Electrospray Ionization Ion Trap Mass Spectrometry and Density Functional Theory. *J. Phys. Chem. A* **2011**, *115* (15), 3497−3508.
(21) Wang, C.-Z.; Shi, W.-Q.; Lan, J.-H.; Zhao, Y.-L.; Wei, Y.-Z.; Chai, Z.-F. Complexation Behavior of Eu(III) and Am(III) with CMPO and Ph_2CMPO Ligands: Insights from Density Functional Theory. *Inorg. Chem.* **2013**, *52* (19), 10904−10911.
(22) Wang, C.-Z.; Lan, J.-H.; Zhao, Y.-L.; Chai, Z.-F.; Wei, Y.-Z.; Shi, W.-Q. Density Functional Theory Studies of UO_2^{2+} and NpO_2^+ Complexes with Carbamoylmethylphosphine Oxide Ligands. *Inorg. Chem.* **2013**, *52* (1), 196−203.
(23) Bühl, M.; Sieffert, N.; Chaumont, A.; Wipff, G. Water versus Acetonitrile Coordination to Uranyl. Density Functional Study of Cooperative Polarization Effects in Solution. *Inorg. Chem.* **2011**, *50* (1), 299−308.
(24) Bernardo, P. D.; Zanonato, P. L.; Benetollo, F.; Melchior, A.; Tolazzi, M.; Rao, L. Energetics and Structure of Uranium(VI)−Acetate Complexes in Dimethyl Sulfoxide. *Inorg. Chem.* **2012**, *51* (16), 9045−9055.
(25) Bühl, M.; Sieffert, N.; Chaumont, A.; Wipff, G.. Water versus Acetonitrile Coordination to Uranyl. Effect of Chloride Ligands. *Inorg. Chem.* **2012**, *51* (3), 1943−1952.
(26) Ziegler, T.; Autschbach, J. Theoretical Methods of Potential Use for Studies of Inorganic Reaction Mechanisms. *Chem. Rev.* **2005**, *105* (6), 2695−2722.
(27) Benay, G.; Wipff, G Liquid−Liquid Extraction of Uranyl by an Amide Ligand: Interfacial Features Studied by MD and PMF Simulations. *J. Phys. Chem. B* **2013**, *117* (24), 7399−7415.
(28) Jackson, V. E.; Gutowski, K. E.; Dixon, D. A. Density Functional Theory Study of the Complexation of the Uranyl-Dication with Anionic Phosphate Ligands with and without Water Molecules. *J. Phys. Chem. A* **2013**, *117* (36), 8939−8957.
(29) Vallet, V.; Wahlgren, U.; Grent, I. Probing the Nature of Chemical Bonding in Uranyl(VI) Complexes with Quantum Chemical Methods. *J. Phys. Chem. A* **2012**, *116* (50), 12373−12380.
(30) Gupta, K. K.; Manchanda, V. K.; Subramanian, M. S.; Singh, R. K. Solvent Extraction Studies On U(VI), Pu(IV), And Fission Products Using *N,N*-dihexyloctanamide. *Solvent Extr. Ion Exch.* **2000**, *18* (2), 273−292.
(31) Thiollet, G.; Musikas, C. Synthesis and uses of the amides extractants. *Solvent Extr. Ion Exch.* **1989**, *7*, 813−827.
(32) Becke, A. D. Density-Functional Exchange-Energy Approximation with Correct Asymptotic Behavior. *Phys. Rev. A* **1988**, *38*, 3098−3100.
(33) Perdew, J. P. Density-Functional Approximation for the Correlation Energy of the Inhomogeneous Electron Gas. *Phys. Rev. B* **1986**, *33*, 8822−8824.
(34) Weigend, F.; Ahlrichs, R. Balanced Basis Sets of Split Valence, Triple Zeta Valence and Quadruple Zeta Valence Quality for H to Rn: Design and Assessment of Accuracy. *Phys. Chem. Chem. Phys.* **2005**, *7*, 3297−3305.
(35) Becke, A. D. Density-Functional Thermo chemistry. III. The Role of Exact Exchange. *J. Chem. Phys.* **1993**, *98*, 5648−5652.
(36) Lee, C.; Yang, W.; Parr, R. G. Development of the Colle-Salvetti Correlation-Energy Formula into a Functional of the Electron Density. *Phys. Rev. B* **1988**, *37*, 785−789.
(37) Schaefer, A.; Horn, H.; Ahlrichs, R. Fully Optimized Contracted Gaussian Basis Sets for Atoms Li to Kr. *J. Chem. Phys.* **1992**, *97*, 2571−2577.
(38) Schaefer, A.; Huber, C.; Ahlrichs, R. Fully Optimized Contracted Gaussian Basis Sets of Triple Zeta Valence Quality for Atoms Li to Kr. *J. Chem. Phys.* **1994**, *100*, 5829−5835.
(39) Neese, F. *ORCA, An Ab Initio Density Functional and Semiempirical Program Package*; University of Bonn: Germany, 2007
(40) Sundararajan, M.; Campbell, A. J.; Hillier, I. H. Catalytic Cycles for the Reduction of $[UO_2]^{2+}$ by Cytochrome c_7 Proteins Proposed from DFT Calculations. *J. Phys. Chem. A* **2008**, *112*, 4451−4457.
(41) Sundararajan, M. Designing Novel Nanomaterials through Functionalization of Carbon Nanotubes with Supramolecules for Application in Nuclear Waste Management. *Sep. Sci. Technol.* **2013**, *48*, 2391−2396.
(42) Jena, N. K.; Sundararajan, M.; Ghosh, S. K. On the Interaction of Uranyl with Functionalized Fullerenes: A DFT Investigation. *RSC Adv.* **2012**, *2*, 2994−2999.

(43) Sundararajan, M.; Ghosh, S. K. Designing Novel Materials through Functionalization of Carbon Nanotubes for Application in Nuclear Waste Management: Speciation of Uranyl. *J. Phys. Chem. A* **2011**, *115*, 6732−6737.
(44) Sundararajan, M.; Sinha, V.; Bandyopadhyay, T.; Ghosh, S. K. Can Functionalized Cucurbituril Bind Actinyl Cations Efficiently? A Density Functional Theory Based Investigation. *J. Phys. Chem. A* **2012**, *116*, 4388−4395.
(45) Goyal, P. S.; Aswal, V. K. Micellar Structure and Inter-Micelle Interactions in Micellar Solutions: Results of Small Angle Neutron Scattering Studies. *Curr. Sci.* **2001**, *80*, 972−979.
(46) Mahajan, R. K.; Vohra, K. K.; Aswal, V. K. Small Angle Neutron Scattering Measurements of Aggregation Behaviour of Mixed Micelles of Conventional Surfactants with Triblock Polymer L64. *Colloids Surf., A* **2008**, *326*, 48−52.
(47) Cao, Zhiji; Balasubramanian, K. Theoretical Studies Of $UO_2^{2+}(H_2O)_n$, $Npo_2^{+}(H_2O)_n$ and $PuO_2^{2+}(H_2O)_n$ Complexes (n = 4−6) in Aqueous Solution And Gas Phase. *J. Chem. Phys.* **2005**, *123* (114309), 1−12.
(48) de Jong, W. A.; Aprà, E.; Windus, T. L.; Nichols, J. A.; Harrison, R. J.; Gutowski, K. E.; Dixon, D. A. Complexation of the Carbonate, Nitrate, and Acetate Anions with the Uranyl Dication: Density Functional Studies with Relativistic Effective Core Potentials. *J. Phys. Chem. A* **2005**, *109* (50), 11568−11577.
(49) Craw, J. S.; Vincent, M. A.; Hillier, I. H.; Wallwork, A. L. Ab Initio Quantum Chemical Calculations on Uranyl, UO_2^{2+}, Plutonyl, PuO_2^{2+} and their Nitrates and Sulfates. *J. Phys. Chem.* **1995**, *99* (25), 10181−10185.
(50) Servaes, K; Hennig, C.; Billard, I.; Gaillard, C.; Binnemans, K; Görller-Walrand, C; Deun, R. V. Speciation of Uranyl Nitrato Complexes in Acetonitrile and in the Ionic Liquid 1-Butyl-3-methylimidazolium Bis(trifluoromethylsulfonyl)imide. *Eur. J. Inorg. Chem.* **2007**, *32*, 5120−5126.
(51) Allen, P. G.; Bucher, J. J.; Shuh, D. K.; Edelstein, N. M.; Reich, T. Investigation of Aquo and Chloro Complexes of UO_2^{2+}, NpO_2^{+}, Np^{4+}, and Pu^{3+} by X-ray Absorption Fine Structure Spectroscopy. *Inorg. Chem.* **1997**, *36* (21), 4676−4683.
(52) Den Auwer, C.; Charbonnel, M. C.; Presson, M. T.; Madic, C.; Guillaumont, R. XAS Study of Actinide Solvent Extraction Compounds II: $UO_2^{2+}(NO_3)_2L_2$ (with L = Tri-isobutylphosphate \ Tri-*n*-butylphosphate \ Trimethylphosphate and Triphenylphosphate. *Polyhedron* **1998**, *17*, 4507−4517.
(53) Thompson, H. A.; Brown, G. E., Jr.; Parks, G. A. XAFS Spectroscopic Study Of Uranyl Coordination in Solids and Aqueous Solutions. *Am. Mineral.* **1997**, *82*, 483−496.
(54) Bühl, M.; Diss, R; Georges, W. Coordination Environment of Aqueous Uranyl(VI) Ion. *J. Am. Chem. Soc.* **2005**, *127* (39), 13506−13507.
(55) Kerisit, S.; Liu, C. Structure, Kinetics, and Thermodynamics of the Aqueous Uranyl(VI) Cation. *J. Phys. Chem. A* **2013**, *117* (30), 6421−6432.
(56) Ikeda-Ohno, A.; Hennig, C.; Tsushima, S.; Scheinost, A. C.; Bernhard, G.; Yaita, T. Speciation and Structural Study of U(IV) and -(VI) in Perchloric and Nitric Acid Solutions. *Inorg. Chem.* **2009**, *48* (15), 7201−7210.
(57) Odoh, S. O.; Schreckenbach, G. Theoretical Study of the Structural Properties of Plutonium(IV) and (VI) Complexes. *J. Phys. Chem. A* **2011**, *115* (48), 14110−14119.
(58) Vasilchenko, D; Tkachev, S; Baidina, I; Korenev, S. Speciation of Platinum (IV) in Nitric Acid Solutions. *Inorg. Chem.* **2013**, *52* (18), 10532−10451.
(59) Gaunt, A. J.; May, I; Neu, M. P.; Reilly, S. D.; Scott, B. L. Structural and Spectroscopic Characterization of Plutonyl(VI) Nitrate under Acidic Conditions. *Inorg. Chem.* **2011**, *50* (10), 4244−4246.
(60) Adamo, C.; Maldiv, P. A Theoretical Study of Bonding in Lanthanide Trihalides by Density Functional Methods. *J. Phys. Chem. A* **1998**, *102* (34), 6812−6820.
(61) Austin, J. P.; Sundararajan, M.; Vincent, M. A.; Hillier, I. H. The Geometric Structures, Vibrational Frequencies and Redox Properties of the Actinyl Coordination Complexes ($[AnO_2(L)_n]^m$; An = U, Pu, Np; L = H_2O, Cl^-, CO_3^{2-}, $CH_3CO_2^-$, OH^-) in Aqueous Solution, Studied by Density Functional Theory. *Dalton Trans.* **2009**, *30*, 5902−5909.